

# Bihelical magnetic relaxation and large scale magnetic field growth

Eric G. Blackman

Department of Physics & Astronomy and Laboratory for Laser Energetics, University of Rochester, Rochester NY 14627; email: blackman@pas.rochester.edu

(submitted to Physics of Plasmas)

## ABSTRACT

A unified, three-scale system of equations accommodating nonlinear velocity driven helical dynamos, as well as time-dependent relaxation of magnetically dominated uni-helical or bihelical systems is derived and solved herein. When opposite magnetic helicities of equal magnitude are injected on the intermediate and small scales, the large scale magnetic helicity grows kinematically (independent of the magnetic Reynolds number) to equal that on the intermediate scale. For both free and driven relaxation large scale fields are rapidly produced. Subsequently, a dissipation-limited dynamo, driven by growth of small scale kinetic helicity, further amplifies the large scale field. The results are important for astrophysical coronae fed with bihelical structures by dynamos in their host rotators. The large scale for the rotator corresponds to the intermediate scale for the corona. That bihelical magnetic relaxation can produce global scale fields may help to explain the formation of astrophysical coronal holes and magnetohydrodynamic outflows.

PACS codes: 52.30.Cv, 95.30.Qd, 52.65Kj, 96.60.Pb, 98.35.Eg, 98.62Mx

## I. Introduction

### A. Background

Large scale helical dynamo theory provides a framework for modeling the in situ origin of large-scale magnetic field growth in planets, stars, and galaxies<sup>1–4</sup> and has also been invoked to explain the sustenance of fields in fusion devices.<sup>5–14</sup> Much of the associated dynamo research can be divided into (1) that which parameterizes the nonlinearities in an effort to practically model the field evolution of specific objects or systems, and (2)

that aimed at identifying the physical principles of the nonlinear dynamo by dynamically including the mutual backreaction between the field and velocities for simplified systems.

Progress in understanding the nonlinear helical field growth and saturation has resulted from a combination of numerical and analytic work that dynamically incorporates magnetic helicity evolution.<sup>15–22</sup> Analytic models<sup>19–24</sup> employing a discrete number of scales and including the backreaction of the field growth on the turbulent velocity have shown that for kinetic helicity driven dynamos, the build up of small scale magnetic helicity ultimately quenches the large scale field growth, in agreement with numerical simulations.<sup>18–26</sup> A two-scale nonlinear theory of large scale field growth from a dynamo driven by small scale magnetic helicity fluctuations rather than kinetic helicity fluctuations has also been developed.<sup>13</sup> In this case the kinetic helicity becomes the quenching agent rather than the growth driver. Like the velocity-driven helical dynamo, such magnetically driven helical dynamos thrive on a finite turbulent electromotive force in Ohm’s law.

A magnetically driven helical dynamo can also be described as “dynamical magnetic relaxation.” Magnetic relaxation describes the process by which magnetic structures in magnetic pressure dominated environments evolve to their equilibrium states. The fully relaxed state is the Taylor state,<sup>28</sup> determined by minimizing the magnetic energy subject to the constraint that magnetic helicity is conserved. The result is a force-free helical configuration with the field relaxing to the largest scale available, subject to boundary conditions. However, Taylor’s theory by itself is not a dynamical theory since it does not provide a time-dependent description of how the large scale magnetic helicity evolves. A time-dependent theory that also includes velocity and fluctuations is required.

In fusion devices, where the plasma is magnetically dominated, the word “dynamo” is typically used to describe a magnetically dominated dynamo in which magnetic flux is converted from toroidal to poloidal (or vice versa), increase the scale of the field, and sustain a strong magnetic flux against microphysical dissipation.<sup>5–14</sup> Detailed studies of these dynamos focus on the instabilities that drive the fluctuations (tearing modes) as well as the subsequent relaxation, conversion and sustenance of the magnetic flux. The full boundary value problem can be solved for specific configurations.

Similar magnetically driven dynamos are likely an important part of the generation of large scale astrophysical fields that mediate coronal holes and magnetohydrodynamic (MHD) jets in astrophysics. The analogy can be drawn between spheromak or reversed-field pinch formation<sup>12</sup> and coronal field relaxation: The laboratory configurations form because the injection of magnetic helicity into a system takes the system away from the relaxed state, but also drives tearing mode fluctuations that yield a finite turbulent electromotive force. This in turn drives the system to to a new relaxed state. In astrophysical coronae

the situation is similar. The helical field produced by a velocity driven dynamo inside of a rotator is buoyantly fed from below into the corona. This takes the magnetically dominated corona away from the relaxed state initially, but fluctuations arise in which the system is then driven back to a relaxed state. The corona therefore acts as the “laboratory” plasma volume, injected with helicity from below. In the astrophysical case, the injection occurs not at one site, but throughout the coronal-surface boundary. While each of the individual injection sites (flux tubes) would be analogous to a single laboratory configuration if the twists are injected along the tube, each tube can also open up to even larger scales by mutual interaction. In this way, magnetic energy can appear on scales even larger than those on which the field was originally present. This is a difference between the laboratory and astrophysical cases.

## B. Astrophysical motivation for bihelical relaxation

Magnetically driven dynamos are important for a wide range of astrophysical coronae because all coronae of turbulent astrophysical rotators (the sun, stars, and accretion disks) are likely magnetically dominated. For the solar corona,<sup>29</sup> observations support the basic paradigm that particle acceleration and heating result from extraction of coronal magnetic energy via reconnection or wave dissipation.<sup>30, 31</sup> The coronal magnetic fields come from magnetic loops produced within the sun that are injected into the corona. Because the field polarity reverses every 11 years, these loops could not have been merely the residue of the accreted interstellar field. The sun also has much larger scale (“open”) fields in coronal holes along which the solar wind propagates. These fields also reverse during the solar cycle, again highlighting that they are not simply the result of flux freezing from the sun’s formation. That the geometry and topology of smaller bipolar structures evolve to produce global structures in the solar cycle can be modeled empirically.<sup>32</sup>

Accretion disk coronae likely involve similar processes. Non-thermal emission and flares from accreting stars or black holes are also naturally explained by the emergence of magnetic fields from the turbulent plasma below.<sup>33–36</sup> By analogy to the sun, disk fields supplied to its corona can open up. Because accretion disks are “fast rotators” (as are young X-ray luminous stars<sup>37</sup>) the open field lines are not only the track along which outflows propagate, but can act as a drive belt to extract the rotational energy in the disk (or young star) supplied by accretion. Conversion of the accretion energy flux into Poynting flux can drive the observed outflows.<sup>40–47</sup> Though particular MHD models differ as to how far above the disk the outflows are carried as Poynting flux,<sup>40, 47</sup> they all involve large scale fields and collectively offer the most viable jet/outflow paradigm for a range of accretion engines.

MHD jet/outflow studies typically impose the global field anchored in the turbulent rotator as an initial condition, and then allow the system to evolve or consider the steady state.<sup>40–46</sup> Because field reversal cycles cannot be directly measured in accretion disks, it is not as straightforward as it is for the sun to directly determine whether the large scale fields are accreted or produced in situ. But difficulties in accreting flux in a thin turbulent disk<sup>38,39</sup> and the fact that the solar corona produces large scale global fields in situ provide reasons to believe that in situ production in disk coronae is ongoing. The supply of magnetic energy to a corona is directly supported by 3-D MHD simulations,<sup>48</sup> but the self-consistent generation of large scale flux still needs further study.

In the standard use of helical dynamos to generate large scale astrophysical fields, an initially weak field is assumed and the growth of the large scale field is studied for given a choice of velocity driving and global boundary conditions.<sup>4,45,46,49–51</sup> While this approach applies inside the rotator, it hides an important aspect of the large scale field generation in the corona. The large scale coronal fields might be more appropriately described as the second phase of a two-phase process: (1) In the first phase, a velocity driven helical dynamo generates large scale fields inside the rotator. The field produced then emerges into the corona. (In order for buoyancy to beat shredding for a disk, a helical dynamo within the rotator seems to be required because non-helical turbulent amplification produces structures that are dissipated before they can rise significantly<sup>39</sup>.) (2) Because the “large” scale field produced by the velocity driven dynamo in the disk is of “intermediate” scale with respect to the corona, it must incur further relaxation to open up to the global scales required by holes and outflows—just as we see in the sun. However, this relaxation occurs in an already magnetically dominated environment, so phase (2), just discussed, is indeed a magnetically dominated dynamo. Because magnetic helicity conservation implies that any nonlinear dynamo in the rotator below produces helical fields of opposite signs on different scales,<sup>15–23</sup> (see Fig. 1 of Ref. 23 for an illustration) the question becomes: Is a net global large scale field produced when injected with bihelical fields that supply a zero net helicity?

### **C. Present aim: closed time-dependent theory, not detailed boundary value study**

Unlike the laboratory dynamo, the astrophysical coronal dynamo involves multiple helicity injection sites (i.e. each buoyant twisted flux tube) rather than a single injection (helicity injection along the mean field.). Nevertheless, in a real corona, like in a laboratory configuration, the global magnetic relaxation will result from current instabilities instigated by the magnetic helicity injection.<sup>12, 27</sup> Indeed, a full treatment of coronal bihelical magnetic

relaxation will ultimately require boundary value studies. However, much insight into the basic nonlinear effects of magnetic helicity transfer and velocity backreaction can be gained using a minimalist mean field approach without a detailed modeling of the tearing modes that drive the fluctuations. Rather than a detailed boundary value problem, I consider a simpler problem in which the scale magnetic helicity is driven into the system quasi-isotropically at the intermediate and small scales and the subsequent growth at the large scale calculated. This is directly analogous to the approach used to study nonlinear principles of velocity driven helical dynamos, and has led to significant progress in reconciling results from analytic treatments and numerical simulations.<sup>15, 18, 20, 25</sup> Keeping the set-up simple (a closed system driven quasi-isotropically with kinetic or magnetic helicity fluctuations), facilitates calculation of how much relaxation occurs on dynamical vs. dissipative time scales, the strength of the backreaction on the relaxation from velocity fluctuation growth, and the properties of the saturated state.

Toward this end, I derive and solve a set of equations that dynamically models the time evolution of a system injected with bihelicity (opposite signs of magnetic helicities on different scales) to determine the extent of the magnetic helicity generation on even larger scales. The system is magnetically dominated in the sense that the energy injected into the system is initially entirely magnetic, and the total magnetic energy (summed over all scales) remains dominant throughout the calculations even when the velocity fluctuations grow. The time dependent evolution requires a three-scale nonlinear theory. The nonlinearity arises because the magnetic helicity equations are coupled to dynamically to equations for the velocity fluctuations. The latter are generated by the magnetically dominated system on its journey to the relaxed state.

In Sec. II, I derive the equations and collect them in dimensionless form. In Sec. III, I solve the equations and discuss the solutions for the following cases: (1) driven bihelical magnetic relaxation, where the system is continuously driven with oppositely signed magnetic helicities on different scales; (2) kinetic helicity driven dynamo, where the system is continuously driven with kinetic helicity only on the intermediate scale; (3) uni-helical magnetic relaxation, where the system is continuously driven with 1 sign of magnetic helicity only on the intermediate scale; (4) free bihelical magnetic relaxation, where the system is initially injected with oppositely signed magnetic helicities on the intermediate and small scales but with no subsequent driving. In Sec. IV, I summarize the results and the implications.

## II. Equations for bihelical magnetic relaxation

In this section, the generalized set of equations that can describe both kinetic helicity and magnetic helicity driven dynamos is derived.

### A. Magnetic helicity equations

I assume that there are 3 scales on which magnetic helicity can reside, defined such that their wave numbers satisfy  $k_3 > k_2 > k_1 > 0$ . I take  $\overline{\mathbf{B}}$ ,  $\overline{\mathbf{A}}$ , and  $\overline{\mathbf{E}}$  to be the components of the magnetic field  $\mathbf{B}$ , vector potential  $\mathbf{A}$ , and electric field  $\mathbf{E}$  that vary on the scale  $k_1^{-1}$ . The respective quantities on scales  $k_2^{-1}$  and  $k_3^{-1}$  will be labeled with subscripts 2 and 3 respectively.

In a closed or global volume, the total magnetic helicity,  $H = \langle \mathbf{A} \cdot \mathbf{B} \rangle$ , satisfies<sup>1,53,54</sup>

$$\partial_t H = -2\langle \mathbf{E} \cdot \mathbf{B} \rangle, \quad (1)$$

where  $\mathbf{E} = -\partial_t \mathbf{A} - \nabla \phi$ ,  $\phi$  is the scalar potential, and  $\langle \rangle$  indicates a global volume average. Such a conservation formula also applies separately to each scale. That is, using  $\overline{\mathbf{E}} = -\partial_t \overline{\mathbf{A}} - \nabla \overline{\phi}$ ,  $\mathbf{e}_2 = -\partial_t \mathbf{a}_2 - \nabla \phi_2$  and  $\mathbf{e}_3 = -\partial_t \mathbf{a}_3 - \nabla \phi_3$  and dotting with  $\overline{\mathbf{B}}$ ,  $\mathbf{b}_2$  and  $\mathbf{b}_3$  respectively we obtain

$$\partial_t H_1 = -2\langle \overline{\mathbf{E}} \cdot \overline{\mathbf{B}} \rangle \quad (2)$$

$$\partial_t H_2 = -2\langle \mathbf{e}_2 \cdot \mathbf{b}_2 \rangle \quad (3)$$

and

$$\partial_t H_3 = -2\langle \mathbf{e}_3 \cdot \mathbf{b}_3 \rangle, \quad (4)$$

where  $H_1 \equiv \langle \overline{\mathbf{A}} \cdot \overline{\mathbf{B}} \rangle$ ,  $H_2 \equiv \langle \mathbf{a}_2 \cdot \mathbf{b}_2 \rangle$ , and  $H_3 \equiv \langle \mathbf{a}_3 \cdot \mathbf{b}_3 \rangle$ . The expressions for  $\langle \overline{\mathbf{E}} \cdot \overline{\mathbf{B}} \rangle$ ,  $\langle \mathbf{e}_2 \cdot \mathbf{b}_2 \rangle$ , and  $\langle \mathbf{e}_3 \cdot \mathbf{b}_3 \rangle$  are

$$\langle \overline{\mathbf{E}} \cdot \overline{\mathbf{B}} \rangle = -\langle \overline{\mathcal{E}} \cdot \overline{\mathbf{B}} \rangle - \langle \overline{\boldsymbol{\epsilon}} \cdot \overline{\mathbf{B}} \rangle + \lambda \langle \overline{\mathbf{J}} \cdot \overline{\mathbf{B}} \rangle \quad (5)$$

$$\langle \mathbf{e}_2 \cdot \mathbf{b}_2 \rangle = \langle \overline{\mathcal{E}} \cdot \overline{\mathbf{B}} \rangle - \langle \boldsymbol{\epsilon}_2 \cdot \mathbf{b}_2 \rangle + \lambda \langle \mathbf{j}_2 \cdot \mathbf{b}_2 \rangle \quad (6)$$

and

$$\langle \mathbf{e}_3 \cdot \mathbf{b}_3 \rangle = \langle \boldsymbol{\epsilon}_2 \cdot \mathbf{b}_2 \rangle + \langle \overline{\boldsymbol{\epsilon}} \cdot \overline{\mathbf{B}} \rangle + \lambda \langle \mathbf{j}_3 \cdot \mathbf{b}_3 \rangle, \quad (7)$$

where  $\lambda$  is the magnetic diffusivity,  $\overline{\mathbf{J}} \equiv \nabla \times \overline{\mathbf{B}}$ ,  $\mathbf{j}_2 \equiv \nabla \times \mathbf{b}_2$  and  $\mathbf{j}_3 \equiv \nabla \times \mathbf{b}_3$  are the normalized currents on the respective scales defined in convenient units,  $\overline{\mathcal{E}} \equiv \overline{\mathbf{v}_2 \times \mathbf{b}_2}$ ,  $\overline{\boldsymbol{\epsilon}} \equiv \overline{\mathbf{v}_3 \times \mathbf{b}_3}$ ,  $\boldsymbol{\epsilon}_2 \equiv (\mathbf{v}_3 \times \mathbf{b}_3)_2$ , and  $(\cdot)_2$  indicates averages which vary on scales  $\geq k_2^{-1}$  and  $\mathbf{v}_2$  and  $\mathbf{v}_3$  are the associated velocities.

Combining equations (2-4) with (5-7) gives

$$\partial_t H_1 = 2\bar{\mathcal{E}}_{||} |H_1^{1/2}| k_1^{1/2} + 2\bar{\epsilon}_{||} |H_1^{1/2}| k_1^{1/2} - 2\lambda k_1^2 H_1 \quad (8)$$

$$\partial_t H_2 = -2\bar{\mathcal{E}}_{||} |H_1^{1/2}| k_1^{1/2} + 2\epsilon_{2||} |H_2^{1/2}| k_1^{1/2} - 2\lambda k_2^2 H_2 \quad (9)$$

and

$$\partial_t H_3 = -2\bar{\mathcal{E}}_{||} |H_1^{1/2}| k_1^{1/2} - 2\epsilon_{2||} |H_2^{1/2}| k_1^{1/2} - 2\lambda k_3^2 H_3, \quad (10)$$

where  $\bar{\mathcal{E}}_{||} \equiv \bar{\mathcal{E}} \cdot \frac{\bar{\mathbf{B}}}{|\bar{\mathbf{B}}|}$ ,  $\bar{\epsilon}_{||} \equiv \bar{\epsilon} \cdot \frac{\bar{\mathbf{B}}}{|\bar{\mathbf{B}}|}$ , and  $\epsilon_{2||} \equiv \epsilon_2 \cdot \frac{\mathbf{b}_2}{|\mathbf{b}_2|}$ . Here the three-scale approach has been used to write  $\langle \bar{\mathbf{J}} \cdot \bar{\mathbf{B}} \rangle = k_1^2 H_1$ ,  $\langle \mathbf{j}_2 \cdot \mathbf{b}_2 \rangle = k_2^2 H_2$ , and  $\langle \mathbf{j}_3 \cdot \mathbf{b}_3 \rangle = k_3^2 H_3$ , and maximal helicity has been assumed so that  $\langle \bar{\mathbf{B}}^2 \rangle = k_1^2 H_1$ ,  $\langle \mathbf{b}_2^2 \rangle = k_2^2 H_2$ ,  $\langle \mathbf{b}_3^2 \rangle = k_3^2 H_3$ .

## B. Time-dependent electromotive force equations

A dynamical nonlinear helical dynamo theory should include<sup>16,20</sup> the time evolution of  $\bar{\mathcal{E}}$  and by generalization to three scales, also the time evolution for  $\bar{\epsilon}$ , and  $\epsilon_2$ . Of primary interest are the specific components  $\bar{\mathcal{E}}_{||}$ ,  $\bar{\epsilon}_{||}$  and  $\epsilon_{2||}$ . We therefore have

$$\partial_t \bar{\mathcal{E}}_{||} = \langle \partial_t \mathbf{v}_2 \times \mathbf{b}_2 \rangle \cdot \frac{\bar{\mathbf{B}}}{|\bar{\mathbf{B}}|} + \langle \mathbf{v}_2 \times \partial_t \mathbf{b}_2 \rangle \cdot \frac{\bar{\mathbf{B}}}{|\bar{\mathbf{B}}|} + \bar{\mathcal{E}} \cdot \partial_t \frac{\bar{\mathbf{B}}}{|\bar{\mathbf{B}}|}, \quad (11)$$

$$\partial_t \bar{\epsilon}_{||} = \langle \partial_t \mathbf{v}_3 \times \mathbf{b}_3 \rangle \cdot \frac{\bar{\mathbf{B}}}{|\bar{\mathbf{B}}|} + \langle \mathbf{v}_3 \times \partial_t \mathbf{b}_3 \rangle \cdot \frac{\bar{\mathbf{B}}}{|\bar{\mathbf{B}}|} + \bar{\epsilon} \cdot \partial_t \frac{\bar{\mathbf{B}}}{|\bar{\mathbf{B}}|} \quad (12)$$

and

$$\partial_t \epsilon_{2||} = (\partial_t \mathbf{v}_3 \times \mathbf{b}_3)_2 \cdot \frac{\mathbf{b}_2}{|\mathbf{b}_2|} + (\mathbf{v}_3 \times \partial_t \mathbf{b}_3)_2 \cdot \frac{\mathbf{b}_2}{|\mathbf{b}_2|} + \epsilon_2 \cdot \partial_t \frac{\mathbf{b}_2}{|\mathbf{b}_2|} \quad (13)$$

To proceed, we need equations for  $\partial_t \mathbf{b}_2$ ,  $\partial_t \mathbf{b}_3$ ,  $\partial_t \mathbf{v}_2$ , and  $\partial_t \mathbf{v}_3$ , which come from the magnetic induction equation

$$\partial_t \mathbf{B} = \nabla \times (\mathbf{v} \times \mathbf{B}) + \lambda \nabla^2 \mathbf{B}, \quad (14)$$

and the incompressible Navier-Stokes equation

$$\partial_t \mathbf{v} = \mathbf{v} \times \boldsymbol{\omega} - \nabla(P + \mathbf{v}^2/2) + \mathbf{J} \times \mathbf{B} + \nu \nabla^2 \mathbf{v}, \quad (15)$$

where  $P$  is the thermal pressure, and  $\boldsymbol{\omega} \equiv \nabla \times \mathbf{v}$ . Because there are multiple fluctuation scales ( $k_2^{-1}$  and  $k_3^{-1}$ ), we must perform multiple averaging. To obtain the equations for quantities with subscript 2 and 3 note that

$$\partial_t \mathbf{b}_2 + \partial_t \mathbf{b}_3 = (\partial_t \mathbf{B} - \partial_t \bar{\mathbf{B}}), \quad (16)$$

so that

$$\partial_t \mathbf{b}_2 = (\partial_t \mathbf{B} - \partial_t \bar{\mathbf{B}})_2, \quad (17)$$

and

$$\partial_t \mathbf{b}_3 = (\partial_t \mathbf{B} - \partial_t \bar{\mathbf{B}}) - (\partial_t \mathbf{B} - \partial_t \bar{\mathbf{B}})_2. \quad (18)$$

The analogous relations apply for  $\partial_t \mathbf{v}_2$  and  $\partial_t \mathbf{v}_3$ , with the simplification that  $\partial_t \bar{\mathbf{V}} = 0$  for the present calculation. Thus

$$\partial_t \mathbf{v}_2 + \partial_t \mathbf{v}_3 = \partial_t \mathbf{v}, \quad (19)$$

so that

$$\partial_t \mathbf{v}_2 = (\partial_t \mathbf{v})_2, \quad (20)$$

and

$$\partial_t \mathbf{v}_3 = \partial_t \mathbf{v} - (\partial_t \mathbf{v})_2. \quad (21)$$

After some algebra, applying this procedure to (14) and (15) gives

$$\partial_t \mathbf{b}_2 = \nabla \times (\mathbf{v}_2 \times \bar{\mathbf{B}}) + \nabla \times (\mathbf{v}_2 \times \mathbf{b}_2)_2 + \nabla \times (\mathbf{v}_3 \times \mathbf{b}_3)_2 + \lambda \nabla^2 \mathbf{b}_2 + \mathbf{f}_{b2}, \quad (22)$$

$$\partial_t \mathbf{b}_3 = \nabla \times (\mathbf{v}_2 \times \mathbf{b}_3) + \nabla \times (\mathbf{v}_3 \times \mathbf{b}_2) + \nabla \times (\mathbf{v}_3 \times \bar{\mathbf{B}}) + \nabla \times (\mathbf{v}_3 \times \mathbf{b}_3)_3 + \lambda \nabla^2 \mathbf{b}_3 + \mathbf{f}_{b3}, \quad (23)$$

$$(\partial_t \mathbf{v}_2)_i = \Pi_{ij} (\bar{\mathbf{B}} \cdot \nabla \mathbf{b}_2 + \mathbf{b}_2 \cdot \nabla \bar{\mathbf{B}})_j + \nu (\nabla^2 \mathbf{v}_2)_i + \mathbf{f}_{v2}, \quad (24)$$

and

$$(\partial_t \mathbf{v}_3)_i = \Pi_{ij} (\bar{\mathbf{B}} \cdot \nabla \mathbf{b}_3 + \mathbf{b}_3 \cdot \nabla \bar{\mathbf{B}} + \mathbf{b}_2 \cdot \nabla \mathbf{b}_3 + \mathbf{b}_3 \cdot \nabla \mathbf{b}_2)_j + \nu (\nabla^2 \mathbf{v}_3)_i + \mathbf{f}_{v3}, \quad (25)$$

where  $\nu$  is the viscosity,  $\mathbf{f}_{b2}$  and  $\mathbf{f}_{b3}$ , are forcing functions assumed not to correlate with  $\mathbf{v}_1, \mathbf{v}_2$ , and  $\mathbf{f}_{v2}$  and  $\mathbf{f}_{v3}$  are forcing functions assumed not to correlate with  $\mathbf{b}_2, \mathbf{b}_3$ . The projection operator  $\Pi_{ij} \equiv \left( \delta_{ij} - \frac{\nabla_i \nabla_j}{\nabla^2} \right)$  comes from taking the divergence of the velocity equation to solve for the total pressure of incompressible flow.

In deriving (17-25) and in subsequent manipulations, the following important simplifying assumptions are made: (1) Mixed correlations between quantities of widely separated scales are assumed small. Thus I ignore terms of the form e.g.  $\langle \mathbf{j}_2 \cdot \mathbf{b}_3 \rangle$ . (Note however that e.g.  $\mathbf{j}_2 \cdot \mathbf{b}_3 \neq 0$ ; only when put in brackets is the assumption applied.) (2) The magnetic field or velocities on a given scale are assumed to be fully helical, so that specifically  $\mathbf{v}_3 \times \boldsymbol{\omega}_3 \simeq \mathbf{v}_2 \times \boldsymbol{\omega}_2 \simeq \bar{\mathbf{V}} \times (\nabla \times \bar{\mathbf{V}}) \simeq \mathbf{j}_3 \times \mathbf{b}_3 \simeq \mathbf{j}_2 \times \mathbf{b}_2 \simeq \bar{\mathbf{J}} \times \bar{\mathbf{B}} \simeq 0$ . This is not as restrictive as it might appear because the mixed quantities e.g.  $\mathbf{j}_2 \times \mathbf{b}_3$  are not assumed to vanish and thus non-linear couplings and transfer between scales are included.



(3) Cross helicities are ignored (e.g. pseudo-scalar mixed correlations between  $\mathbf{v}$  and  $\mathbf{b}$  such as  $\langle \mathbf{b} \cdot \mathbf{v} \rangle$ ). (4) It is assumed that terms involving the correlation of products of separate quantities averaged over the intermediate scale can be factored into two global correlations. That is,  $\langle (\mathbf{j}_3 \cdot \mathbf{b}_3)_2 b_2^2 \rangle \simeq \langle \mathbf{j}_3 \cdot \mathbf{b}_3 \rangle \langle b_2^2 \rangle$  and  $\langle (\mathbf{v}_3 \cdot \boldsymbol{\omega}_3)_2 b_2^2 \rangle \simeq \langle \mathbf{v}_3 \cdot \boldsymbol{\omega}_3 \rangle \langle b_2^2 \rangle$ .

Armed with these assumptions, Eqs. (22-25) must now be used in Eqs. (11) and (13). Eqs. (22) and (23) are required for the third terms in (11) and (13). These terms can be computed in configuration space by direct substitution of the latter two equations into the former. Eqs. (24) and (25) are required for the second terms in (11) and (13). These terms are computed by Fourier transforms,<sup>10,20</sup> and triple correlations are also retained by use of the “minimal  $\tau$ ” closure<sup>20</sup> (which obviates the first order smoothing approximation) by approximating the triple correlations as the product of the respective electromotive force divided by a damping time scale. Applying this closure here, the triple correlation arising from the fifth term of (23), when input into the third term of (13), contributes a term of the form  $-\bar{\epsilon}_{||}|v_3 k_3|$ , and the third and fourth terms of (22) when plugged into the third term of (11) contribute terms of the form  $-\bar{\mathcal{E}}_{||}|v_2 k_2|$ , and  $-\bar{\epsilon}_{||}|v_3 k_3|$  respectively. It should also be noted that the last terms of (11) and (13) respectively will also be included in these damping terms. The coefficients of the damping terms can in principle be taken to be different from unity<sup>20</sup> but this is not considered further here.

Using the above approximations and plowing through the algebra that arises from plugging Eqs. (22-25) into (11-13) gives

$$\partial_t \bar{\mathcal{E}}_{||} = \left( k_2^2 H_2 - H_2^V \right) \frac{|H_1^{1/2}| k_1^{1/2}}{3} - \frac{H_2^V}{3} \frac{k_1^{3/2}}{k_2} \frac{H_1}{|H_1^{1/2}|} - \bar{\mathcal{E}}_{||} k_2^2 (v_2/k_2 + \lambda + \nu) - \epsilon_{2||} k_2 v_2, \quad (26)$$

$$\partial_t \bar{\epsilon}_{||} = \left( k_3^2 H_3 - H_3^V \right) \frac{|H_1^{1/2}| k_1^{1/2}}{3} - \frac{H_3^V}{3} \frac{k_1^{3/2}}{k_3} \frac{H_1}{|H_1^{1/2}|} - \bar{\epsilon}_{||} k_3^2 (v_3/k_3 + \lambda + \nu), \quad (27)$$

and

$$\partial_t \epsilon_{2||} = \left( k_3^2 H_3 - H_3^V \right) \frac{|H_2^{1/2}| k_2^{1/2}}{3} - \frac{H_3^V}{3} \frac{k_2^{3/2}}{k_3} \frac{H_2}{|H_2^{1/2}|} - \epsilon_{2||} k_3^2 (v_3/k_3 + \lambda + \nu), \quad (28)$$

where  $H_2^V \equiv \langle \mathbf{v}_2 \cdot \boldsymbol{\omega}_2 \rangle$  and  $H_3^V \equiv \langle \mathbf{v}_3 \cdot \boldsymbol{\omega}_3 \rangle$  are the kinetic helicities associated with the respective scales.

### C. Kinetic helicity equations

To close the set of equations, we need dynamical equations for  $H_2^V$  and  $H_3^V$ . Using (20) and (21) in (15) to obtain equations for  $\partial_t \mathbf{v}_2$ ,  $\partial_t \boldsymbol{\omega}_2$ ,  $\partial_t \mathbf{v}_3$  and  $\partial_t \boldsymbol{\omega}_3$ , ignoring total divergences

inside of averaging brackets and using the assumptions discussed below (25) we obtain

$$\partial_t H_2^V = 2\langle \bar{\mathbf{J}} \cdot (\mathbf{b}_2 \times \boldsymbol{\omega}_2) \rangle + 2\langle \bar{\mathbf{B}} \cdot (\boldsymbol{\omega}_2 \times \mathbf{j}_2) \rangle \simeq 2(k_2^2 - k_1 k_2) \langle \bar{\boldsymbol{\epsilon}} \cdot \mathbf{B} \rangle - 2k_2^2 \nu H_2^V \quad (29)$$

and

$$\begin{aligned} \partial_t H_3^V &= 2\langle \bar{\mathbf{J}} \cdot (\mathbf{b}_3 \times \boldsymbol{\omega}_3) \rangle + 2\langle \bar{\mathbf{B}} \cdot (\boldsymbol{\omega}_3 \times \mathbf{j}_3) \rangle + 2\langle \mathbf{j}_2 \cdot (\mathbf{b}_3 \times \boldsymbol{\omega}_3) \rangle + 2\langle \mathbf{b}_2 \cdot (\boldsymbol{\omega}_3 \times \mathbf{j}_3) \rangle \\ &\simeq 2(k_3^2 - k_1 k_3) \langle \bar{\boldsymbol{\epsilon}} \cdot \bar{\mathbf{B}} \rangle + 2(k_3^2 - k_2 k_3) \langle \boldsymbol{\epsilon}_2 n \cdot \mathbf{b}_2 \rangle - 2k_3^2 \nu H_3^V, \end{aligned} \quad (30)$$

where the latter similarities in (29) and (30) follow from maximally helical assumptions  $\mathbf{j}_2 \propto \mathbf{b}_2$ ,  $\boldsymbol{\omega}_2 \propto \mathbf{v}_2$ ,  $\mathbf{j}_3 \propto \mathbf{b}_3$ , and  $\boldsymbol{\omega}_3 \propto \mathbf{v}_3$ , and the assumptions that  $\frac{\boldsymbol{\omega}_2 \cdot \mathbf{v}_2}{|\boldsymbol{\omega}_2||\mathbf{v}_2|} = \frac{\mathbf{j}_2 \cdot \mathbf{b}_2}{|\mathbf{j}_2||\mathbf{b}_2|}$  and  $\frac{\boldsymbol{\omega}_3 \cdot \mathbf{v}_3}{|\boldsymbol{\omega}_3||\mathbf{v}_3|} = \frac{\mathbf{j}_3 \cdot \mathbf{b}_3}{|\mathbf{j}_3||\mathbf{b}_3|}$ . These latter relations will prove to be self-consistent for the solutions discussed later.

#### D. Aggregate set of equations in dimensionless form to be solved

Before collecting the complete set of equations to be solved, it is useful to add injection and loss terms to the three magnetic helicity equations derived above. Since we will study the evolution of magnetic helicity for a system subject to injection of bihelicity—that is, helicity injected of opposite sign on the scales  $k_2^{-1}$  and  $k_3^{-1}$ —we add terms to the  $H_2$  and  $H_3$  equations that account for injection (or loss) of magnetic helicity on these respective scales. In addition, if the system is a corona of finite volume, large scale fields therein might be able to escape as Poynting flux. While the injection terms just described can be used to combine injection and loss for  $H_2$  and  $H_3$ , for  $H_1$  I add a distinct Poynting loss term  $\propto \bar{\mathbf{V}}_A H_1 k_1 \sim H_1^{3/2} k_1^{1/2}$ , where  $\bar{\mathbf{V}}_A = \bar{\mathbf{B}}$  is the Alfvén speed associated with  $\bar{\mathbf{B}}$  (recall that magnetic fields are written in Alfvén units herein). (When losses are included, the magnetic helicities should be re-interpreted as gauge invariant relative helicities<sup>54</sup> with respect to a background potential field, but the basic formalism herein does not change significantly.)

For completeness, I also include injection (or loss) terms in the  $H_2^V$  and  $H_3^V$  equations. Use of the injection term for  $H_2^V$  will help illustrate the relation of the present study to the 2-scale solution of the kinetic helicity driven dynamo.<sup>20</sup>

To write the needed equations in dimensionless form, define  $h_1 \equiv H_1/|\tilde{H}_{2,0}|$ ,  $h_2 \equiv H_2/|\tilde{H}_{2,0}|$ ,  $h_3 \equiv H_3/|\tilde{H}_{2,0}|$ ,  $h_2^V \equiv H_2^V/|k_2^2 \tilde{H}_{2,0}|$ ,  $h_3^V \equiv H_3^V/|k_2^2 \tilde{H}_{2,0}|$ ,  $R_M \equiv \tilde{H}_{2,0}^{1/2}/\lambda k_2^{1/2}$ ,  $R_V \equiv \tilde{H}_{2,0}^{1/2}/\nu k_2^{1/2}$ ,  $\tau \equiv t k_2^3/2\tilde{H}_{2,0}$ ,  $\bar{Q} = \bar{\boldsymbol{\epsilon}}_{||}/k_2 \tilde{H}_{2,0}$ ,  $\bar{q} = \bar{\boldsymbol{\epsilon}}_{||}/k_2 \tilde{H}_{2,0}$ , and  $q_2 = \boldsymbol{\epsilon}_{2||}/k_2 \tilde{H}_{2,0}$ , where  $\tilde{H}_{2,0} = H_2(0)$  if magnetic helicity is initially injected and  $\tilde{H}_{2,0} = H_2^V(0)/k_2^2$  if kinetic helicity is initially injected. Using these dimensionless parameters and adding the afore mentioned injection and loss terms, Eqs. (8-10) become

$$\partial_\tau h_1 = 2\bar{Q}|h_1^{1/2}| \left(\frac{k_1}{k_2}\right)^{1/2} + 2\bar{q}|h_1^{1/2}| \left(\frac{k_1}{k_2}\right)^{1/2} - \frac{2h_1}{R_m} \left(\frac{k_1}{k_2}\right)^2 - c_1 |h_1^{3/2}| (k_1/k_2)^{3/2}, \quad (31)$$

$$\partial_\tau h_2 = s_2 - 2\overline{Q}|h_1^{1/2}| \left(\frac{k_1}{k_2}\right)^{1/2} + 2q_2|h_2^{1/2}| - \frac{2h_2}{R_m}, \quad (32)$$

and

$$\partial_\tau h_3 = s_3 - 2\overline{q}|h_1^{1/2}| \left(\frac{k_1}{k_2}\right)^{1/2} - 2q_2|h_2^{1/2}| - \frac{2h_3}{R_m} \left(\frac{k_3}{k_2}\right)^2, \quad (33)$$

where  $c_1$  is a constant parameterizing the Poynting loss term and  $s_1$  and  $s_2$  are the helicity injection terms described in the previous paragraph.

Completing the set of equations using the dimensionless variables defined above, we have for Eqs. (26-28) and (29-30)

$$\partial_\tau \overline{Q} = \frac{1}{3}(h_2 - h_2^V)|h_1^{1/2}| \left(\frac{k_1}{k_2}\right)^{1/2} - \frac{1}{3}|h_2^V| \left(\frac{h_1}{|h_1^{1/2}|}\right) \left(\frac{k_1}{k_2}\right)^{3/2} - \overline{Q} \left(|\sqrt{h_2^V}| + \frac{1}{R_M} + \frac{1}{R_V}\right) - q_2|\sqrt{h_2^V}|, \quad (34)$$

$$\partial_\tau \overline{q} = \frac{1}{3}(h_3 - h_3^V)|h_1^{1/2}| \left(\frac{k_1}{k_2}\right)^{1/2} \left(\frac{k_3}{k_2}\right)^2 - \frac{1}{3}|h_3^V| \left(\frac{h_1}{|h_1^{1/2}|}\right) \left(\frac{k_1}{k_3}\right) \left(\frac{k_1}{k_2}\right)^{1/2} - \overline{q} \frac{k_3^2}{k_2^2} \left(\frac{k_2}{k_3}|\sqrt{h_3^V}| + \frac{1}{R_M} + \frac{1}{R_V}\right), \quad (35)$$

$$\partial_\tau q_2 = \frac{1}{3}(h_3 - h_3^V)|h_2^{1/2}| \left(\frac{k_3}{k_2}\right)^2 - \frac{1}{3}|h_3^V| \left(\frac{h_2}{|h_2^{1/2}|}\right) \left(\frac{k_2}{k_3}\right) - q_2 \frac{k_3^2}{k_2^2} \left(\frac{k_2}{k_3}|\sqrt{h_3^V}| + \frac{1}{R_M} + \frac{1}{R_V}\right), \quad (36)$$

$$\partial_\tau h_2^V = s_2^V + 2\overline{Q}|h_1^{1/2}| \left(\frac{k_1}{k_2}\right)^{1/2} \left(1 - \frac{k_1}{k_2}\right) - \frac{2h_2^V}{R_V}, \quad (37)$$

and

$$\partial_\tau h_3^V = s_3^V + 2 \left(\frac{k_3^2}{k_2^2} - \frac{k_1 k_3}{k_2^2}\right) \overline{q}|h_1^{1/2}| \left(\frac{k_1}{k_2}\right)^{1/2} + 2 \left(\frac{k_3^2}{k_2^2} - \frac{k_3}{k_2}\right) q_2|h_2^{1/2}| - \frac{2h_3^V}{R_V} \left(\frac{k_3}{k_2}\right)^2, \quad (38)$$

where  $s_2^V$  and  $s_3^V$  are the analogous source terms to  $s_2$  and  $s_3$ . Eqs. (31-38) can be solved for  $h_1$ ,  $h_2$ ,  $h_3$ ,  $\overline{Q}$ ,  $\overline{q}$ ,  $q_2$ ,  $h_3^V$ , and  $h_2^V$  as a function of time for a variety of different initial conditions. A few cases are studied below.

### III. Discussion of solutions

Eqs. (31-38) provide a unifying framework for both velocity driven and magnetically driven nonlinear dynamos. They characterize the magnetic and kinetic helicity dynamics for a range of different physical scenarios, depending on the initial conditions. In all cases, below  $k_1 = 1$ ,  $k_2 = 5$  and  $k_3 = 20$ .

### A. Driven dynamical bihelical magnetic relaxation

Consider the case for which  $\partial_t h_3 = \partial_t h_2 = s_2^V = s_3^V = 0$  and  $h_2 = -h_3 = 1$  for all times. This implies continuous injection and removal of oppositely signed magnetic helicities on the intermediate and small scales so as to maintain  $h_2 = -h_3$ . Fig. 1 shows the solutions of Eqs. (31-38) for initial ( $t = 0$ ) values  $h_1(0) = 0.01$ ,  $h_2^V(0) = h_3^V(0) = \overline{Q}(0) = \overline{q}(0) = q_2(0) = 0$ . Fig 1a shows  $h_1$  through the saturated regime and Fig 1b focuses on its early time solution. Fig 1c shows  $h_2$  and  $h_2^V$ , Fig 1d shows  $h_3$  and  $h_3^V$ , Fig. 1e shows  $\overline{Q}$ ,  $\overline{q}$ , and  $q_2$ , and Fig 1f is a diagnostic solution. These are discussed below.

#### 1. Late time regime

To analytically estimate the late time steady state solution for  $h_1$  of Fig 1a, note that from equation (37) in the steady state,  $\overline{Q}$  is inversely proportional to the large quantities  $R_V$  and  $h_1^{1/2}$ . Assuming that  $|\overline{Q}| \ll |\overline{q}|$  and  $|\overline{Q}| \ll |q_2|$  (these will turn out to be valid assumptions), we can then use Eqs. (31), (36), and (38) to find the saturation value of  $h_1$ .

In the steady-state, Eq. (38) gives

$$q_2 \simeq -\overline{q} h_1^{1/2} \left( \frac{k_1}{k_2} \right)^{1/2} \left( \frac{1 - k_1/k_2}{1 - k_2/k_3} \right), \quad (39)$$

assuming that the last term in (38) is small. The fact that  $q_2$  asymptotes to negative values implies that  $h_3 \sim h_3^V$  in (36) due to the growth of  $h_3^V$ . The steady limit of Eq. (36) can then be rearranged to give the approximate relation

$$q_2 \simeq -\frac{1}{3} \frac{k_2^2}{k_3^2}, \quad (40)$$

where we have neglected the  $R_M$  and  $R_V$  terms in that equation as they are small. Combining (39) and (40) gives

$$\overline{q} \simeq \frac{1}{3} \frac{k_2^2}{k_3^2} \left( \frac{h_2}{h_1} \right)^{1/2} \left( \frac{k_2}{k_1} \right)^{1/2} \left( \frac{1 - k_2/k_3}{1 - k_1/k_3} \right). \quad (41)$$

This equation can then be used in the steady-state limit of Eq. (31). Using the earlier assumption that  $|\overline{Q}| \ll |\overline{q}|$ , we then have

$$h_1 \simeq \frac{R_M}{3} \frac{k_2^4}{k_1^2 k_3^2} \left( \frac{1 - k_2/k_3}{1 - k_1/k_3} \right), \quad (42)$$

which provides an excellent approximation to the actual solution at late times. It also shows the insensitivity to  $R_V$ .

The saturated  $h_1 \propto R_M$  in (42), is also exhibited in Fig. 1a. This can be understood as follows:  $h_1$  grows first with the sign of  $h_2$  by direct analogy to unihelical magnetic relaxation,<sup>13</sup> (see also sec. 3.2.2): The magnetic helicity seeks the largest scale available of a given sign. However in the bihelical case, the additional injection of negative  $h_3$  drives the growth of negative  $h_3^V$ . In fact,  $|h_3^V|$  grows to very slightly exceed  $|h_3|$  as seen in Fig. 1d. Then,  $\bar{q}$  becomes slightly positive. This drives additional  $h_1$  growth by an induced kinetic helicity driven dynamo from  $h_3^V$ , by maintaining the  $\bar{q}$  term on the right of (31) at a positive value (long dashed curve in fig 1e). The larger the value of  $R_M$ , the less competitive the last term on the right of (31) is with the  $\bar{q}$  growth term. This explains the  $R_M$  dependence of the saturation value of  $h_1$ .

The above interpretation can be tested by artificially reducing the coupling of  $h_3^V$  to the other equations. This was done to produce the solutions in Fig. 1f by multiplying the entire right side of (38) by  $10^{-6}$ . Notice the significant reduction in the value of  $h_1$  at even relatively early times compared to Fig 1a. In this case, the presence of  $h_3$  acts to damp the growth of  $h_1$  because  $\bar{q}$  remains negative at all times. The two curves in Fig 1e also confirm that it is indeed the  $q_2$  term in (34) that leads to the rapid growth of  $h_1$  in Fig 1a,b since lowering the coefficient on that term lowers the saturated  $h_1$ .

## 2. Early time, kinematic regime

In Fig. 1b, the early time solution for  $h_1$  is shown. The solution is independent of  $R_M$  up to  $h_1 \sim 1$ . At early times, growth of  $h_1$  is dominated by the first term on the right side of (31). The dominant term for the growth of  $h_2^V$  from (37) is very similar and thus the two initially grow at nearly the same rate. However,  $h_2^V$  eventually builds up to a value that stops the growth of  $\bar{Q}$  in (34), after which the latter decays and the growth of  $h_1$  and  $h_2^V$  slows. The decay of  $\bar{Q}$  occurs when the first two terms on the right of (34) approximately balance. Since  $h_2 = 1$ , the critical  $h_2^V$  is  $\sim h_2/(1 + k_1/k_2) \sim 0.83$ . This provides an excellent match to the value of  $h_2^V$  at the end of the kinematic regime shown in Fig 1e. Since the growth rate of  $h_2^V$  is slightly less than that of  $h_1$  due the presence of the  $(1 - k_1/k_2)$  factor in the first term on the right of (37) compared to the first term on the right of (31),  $h_1$  grows a bit larger than  $h_2 \sim 1$  during the kinematic regime. After this time the growth depends on  $R_M$ . Just after the kinematic regime, the  $h_1$  curve for lower  $R_V$  is the higher of the two curves in Fig. 1b. This is because a lower  $R_V$  reduces the kinetic helicity backreaction in  $\bar{Q}$  since the velocity decays faster. However, the two curves eventually cross to produce the

late time solution of Fig. 1a for the reasons discussed in the previous subsection.

The value of  $h_1$  reached during the kinematic regime during bihelical relaxation is approximately the same as that reached in the kinematic regimes of the simpler two-scale uni-helical magnetic relaxation model<sup>13</sup> and the kinetic helicity driven helical dynamo<sup>20</sup> for the similar reason that in these cases, growth of the largest scale helicity is driven by the difference between magnetic and kinetic helicities from the small scale. Driving a two scale system with kinetic (magnetic) or magnetic helicity grows the large scale  $h_1$  rapidly at first, but then the magnetic (kinetic) helicity on the small scale builds up and quenches the growth to dissipation limited rates. As discussed in the previous subsection, the evolution of  $h_1$  differs for bihelical relaxation long after the kinematic regime. Sec. III.B shows how all of these cases are consistent and just depend on the choice of initial conditions.

Finally, a few more comments on Fig. 1c and d: Although curves for both  $R_M = 1000$  and  $R_M = 6000$  are shown in both panels, they overlap at early times when there is no  $R_M$  dependence. Also notice the oscillations in  $h_3^V$ , which damp very quickly, after which  $h_3^V$  remains steady. Remember that the unit of time is defined on the  $k_2^{-1}$  scale. The short evolution time of  $h_3^V$  results from the factors of  $(k_3/k_2)^2 = 16$  in Eq. (38).

### 3. Comparing $k_2 = k_3$ vs $k_3 > k_2$

If  $k_2 = k_3$ , then for the case of Fig. 1 where  $h_2 = -h_3 = 1$ , the net injection of helicity at the scale  $k_2 = k_3$  would be zero and nothing should happen. This has been tested and indeed there is no growth for this case. This highlights that although growth of  $h_1$  can occur when the net injection of  $h_2 + h_3 = 0$ , the two signs of helicity must be injected on sufficiently different scales ( $k_3^2/k_2^2 \gg 1$ ) for non-trivial solutions.

### 4. Inclusion of boundary terms

In Fig.1,  $c_1 = 0$ . Fig. 2 shows the effect of varying  $c_1 > 0$ , to approximate different finite loss rates of  $h_1$ . The result is that the value of  $h_1$  saturates at much lower values than in Fig. 1a, as expected.

### 5. Case of fixed $\partial_t h_2 = -\partial_t h_3 = \text{constant}$

In the previous subsections,  $s_2 = s_3 = 0$  and  $h_2 = 1$  and  $h_3 = -1$  were held constant. The case of constant injection rate, namely  $s_1 = 1$  and  $s_2 = -1$ , is a natural alternative to consider. Solutions for this case also reach a steady state at late times. Higher values of  $h_1$  are obtained in this case than for the fixed  $h_2 = -h_3$  case. I do not discuss this case further here as the implications are similar.

## B. Kinetic helicity driven dynamo and driven uni-helical relaxation

In previous two-scale and three-scale approaches for the kinetic helicity driven dynamo,<sup>20–22</sup> dynamical equations for the kinetic helicity were unnecessary because the kinetic helicity was kept steady. In contrast, the uni-helical relaxation study<sup>13</sup> did include kinetic helicity dynamics but it was a two-scale approach with only 1 sign of injected magnetic helicity. That the equations (31-38) are more general means that they should reduce to these other cases in the appropriate limits.

### 1. Kinetic helicity driven dynamo

If the system is driven steadily with  $h_2^V$  starting with only a seed  $h_1$  and  $h_2 = h_3 \simeq 0$ , then the solution reproduces the non-linear multi-scale helical dynamo<sup>22</sup>, which in turn is consistent with the results of the two-scale version.<sup>20</sup> Fig. 3 shows the resulting solution for  $h_1$ , which represents a simple  $\alpha^2$  dynamo.<sup>18, 20</sup> The rate of growth up to  $h_1 = 1$  is fast and independent of  $R_M$ . The ultimate steady state ratio  $h_1/h_2 = (k_2/k_1)^2 = 25$  to which the solution converges at late times ( $t > R_M k_2/k_1$ ), is also independent of  $R_M$ . This can be seen from solving equations (31) and (32) with  $s_2 = c_1 = \bar{q} = q_2 = 0$  in the steady state).

The rate of approach to the steady state is slower for smaller  $R_M$ . This is because the growth of  $h_1$  for the  $h_2^V$  driven dynamo occurs by segregating opposite signs of magnetic helicity to small and large scales. Growing  $h_1$  larger than  $h_2$  means that  $h_2$  has to dissipate faster than  $h_1$ . The larger the  $R_M$ , the slower the dissipation of  $h_2$ , leading to a smaller  $\bar{Q}$ , and a longer time for  $h_1$  to saturate.

This late-time dependence on  $R_M$  differs from that of  $h_1$  growth in bi-helical magnetic relaxation as discussed in Sec. III.A.1. There, a larger  $R_M$  gave a larger saturation value and a faster growth rate at late times. The difference arises because growing  $h_1$  at late times in that case is not determined by losing small scale magnetic helicity but by maximizing

the effect of the secondary induced  $h_3^V$  driven dynamo. There is no contradiction in the role of  $R_M$  between these two cases because of the difference in the initial conditions.

The saturated value of  $h_1$  depends slightly on the value of turbulent diffusion (the third term of (34)) and its quenching. Different scaling factors for turbulent diffusion were used previously<sup>20, 21</sup> and these differences explain the small difference in the saturation values therein when compared to Fig 3. There is no dynamical quenching of turbulent diffusion in either the present or previous approaches, so here I simply eliminated the extra multiplicative phenomenological factors.

In short, the equations of Sec. 2 fully account for results in the previous studies of the nonlinear  $\alpha^2$  dynamo.

## 2. Unihelical magnetic relaxation

If the system is driven with  $h_2$  but without  $h_3$ , then the growth of  $h_1$  responds just as in unihelical dynamical relaxation.<sup>13</sup> The injected helicity  $h_2$  drives the growth of  $h_1$  by dynamical relaxation. (This is called unihelical relaxation because the helicity is injected with 1 sign at  $h_2$  and the same sign then grows at  $h_1$ .) Fig. 4 shows the growth of  $h_1$ . The kinematic regime proceeds until  $h_1 \sim 1$ , after which the growth of  $h_1$  depends on dissipation. However, unlike the bihelical magnetic relaxation of section 3.1, here the late time saturation value of  $h_1$  depends on the ratio  $R_V/R_M$ . Here  $h_2^V$  plays the role of back reactor, and a larger  $R_V$  means that  $h_2^V$  is more effectively drained, allowing further  $h_1$  growth until saturation. Again note that in the contrasting bihelical case of Fig. 1, the saturation value of  $h_1$  is insensitive to  $R_V$  (for  $R_V \gg 1$ ). There is no contradiction because in that case, both positive and negative signs of magnetic helicity are injected and the  $h_3 = -1$  injection produces an additional  $h_3^V$  driven dynamo through  $\bar{q}$  in (31) that dominates any effect of the suppression of  $\bar{Q}$  at late times.

The important point is that the previously studied case of two-scale unihelical relaxation emerges from the more general equations of Sec. 2 by the appropriate choice of initial conditions.

## C. Free dynamical bihelical magnetic relaxation

In the previous sections, either kinetic or magnetic helicity was assumed to be continuously driven into the system. Here I consider the case where with initial  $h_2(0) = -h_3(0) = 1$  and  $h_1(0) = 0.01$ , but with no subsequent driving or boundary terms,



i.e.  $c_1 = s_2 = s_3 = s_2^V = s_3^V = 0$ . The system is then allowed to freely relax. Results of this case are shown in Fig. 5a-f.

From Fig. 5a and 5b, it is evident that significant growth of  $h_1$  occurs. The kinematic phase (independent of  $R_M$  and  $R_V$ ) ends when  $h_2 \sim h_2^V \sim h_1 \simeq 1/2$  by analogy to free uni-helical relaxation,<sup>13</sup> due to transfer of  $h_2$  to  $h_1$ . Fig. 5b shows that  $h_1 \sim 1/2$  rather than  $h_1 \sim 1$  is reached in the kinematic phase because  $h_2$  also drives the growth of  $h_2^V$ . When  $h_2^V \sim 1/2$ , transfer of  $h_2$  to  $h_1$  is shut down as  $\overline{Q}$  depletes from the decrease in the first term on the right of (34). After the kinematic phase, the  $h_3^V$  induced secondary dynamo described in Sec. III.A takes over to amplify  $h_1$  a bit beyond the kinematic value. Here this has only a small effect because without forcing the system eventually decays.

For larger  $R_M$ , the slower the eventual decay of  $h_1$ . This is as expected from (31), but with the subtle implication that the  $\overline{Q}$  and  $\overline{q}$  terms combine to give a net contribution that does not affect the sensitivity to  $R_M$  from the dissipative term. For fixed  $R_M$  but smaller  $R_V$ , the decay rate of  $h_1$  is the same, but the maximum  $h_1$  reached is smaller. This is evident from comparing the middle and top curves of Fig. 5a and is correlated with the faster depletion of  $h_3^V$  and  $h_3$  in Fig. 5c and 5e for the lower  $R_V$  case. Remember that  $h_3^V$  drives a secondary dynamo that grows  $h_1$  beyond the kinematic regime. As  $R_V$  is decreased,  $h_3^V$  decays faster making this secondary dynamo is less effective. Because  $h_3$ , and thus  $h_3^V$  are not continuously supplied, the secondary dynamo decays and so does  $h_1$ . For arbitrarily larger  $R_V$  than shown in Fig. 5a, the maximum reached by  $h_1$  before it starts to decay is  $h_1 \sim (1 - k_2/k_3) = 0.75 < h_2(0)$ .

The curves for  $h_3$  and  $h_3^V$  indistinguishably overlap in Fig. 5c but a blow up in Fig 5d shows that the  $h_2^V$  curves lie slightly to the right of the  $h_3$  curves. This slight offset is enough to drive the dissipation limited secondary dynamo just described. Fig. 5c also shows that  $h_3^V$  and  $h_3$  deplete faster for smaller  $R_M$ . This is expected from Eqs. (33) and (38) but with the implication that the  $\overline{q}$  and  $\overline{q}_2$  terms combine to give a net contribution that does not contradict the  $R_M$  and  $R_V$  dependence from the dissipative terms.

In contrast to the slower decay of  $h_1$ ,  $h_3$  and  $h_3^V$  with increased  $R_M$ , Fig. 5b. shows that  $h_2$  and  $h_2^V$  actually decay faster with increasing  $R_M$ . At first this may seem counterintuitive but it results because  $q_2$  is negative and decays more slowly with increasing  $R_M$ . Thus the contribution from the  $q_2$  term in (32) acts as a decay term. That this term is larger for larger  $R_M$  is evident from Fig. 5f where the bottom two curves show  $q_2$  for  $R_M = 2000$  and  $R_M = 10000$  respectively. The bottom two curves are close to the asymptotic values for large  $R_M$ . Little change occurs for higher value  $R_M > 10000$  (not shown).

Despite the subtleties, the key point to take away from the free bihelical relaxation

solution is that  $h_1$  grows fast and decays more slowly than  $h_2$  or  $h_3$ . Like the driven case of Sec. III.A, when the system is injected with magnetic helicity of equal magnitude but opposite signs on intermediate and small scales  $k_2^{-1}$  and  $k_3^{-1}$ , significant magnetic helicity grows on the largest  $k_1^{-1}$  scale kinematically. For injected values of  $h_2 = -h_3 = 1$ ,  $h_1$  grows to  $h_1 \sim h_2(0)/2 \sim 1/2$  kinematically and independent of  $h_1(0)$ . The growth time is approximately the Alfvén crossing time of the  $k_1^{-1}$  scale using the injected field strength from  $h_2$ . Unlike the driven case where the maximum  $h_1$  reached at late times is proportional to  $R_M$ , in the free case the maximum post-kinematic  $h_1$  reached for  $R_M \rightarrow \infty$  is  $h_1 \lesssim 1$ . Subsequently,  $h_1$  resistively decays.

The free bihelical relaxation treated in this section is different from that of Ref. (52). There, the system was initially injected with helicity of one sign on the largest scale and the opposite sign on a smaller scale. In contrast, here the helicity is injected on two scales both smaller than the largest scale and helicities on all three scales are allowed to evolve. Once  $h_1$  grows to its maximum and  $h_2$  depletes, the subsequent resistive evolution of  $h_1$  and  $h_3$  acts qualitatively like the relaxation of the random bihelical case of Ref. (52) in that  $h_1$  resistively decays more slowly than  $h_3$ .

#### IV. Summary and Implications

A generalized set of equations that encompasses non-linear velocity driven dynamos as well as magnetically driven dynamos (equivalently, dynamical magnetic relaxation) is derived and solved herein. Previous work focused on these processes separately, but here the different processes are unified into a single set of equations that includes the dynamical evolution of kinetic helicity, magnetic helicity, and the turbulent electromotive forces. Particularly important is that the present approach includes the dynamics of 3 scales: two fluctuation scales in addition to the global scale, rather than just a single fluctuation scale and global scale. This is fruitful because it allows studying bihelical relaxation, the evolution of the helicities on all three scales when helicities of opposite signs are injected on the intermediate and small scale respectively.

Example solutions of the bihelical magnetic relaxation equations reveal that even when a net zero magnetic helicity is supplied to the system by injecting equal and opposite values on sufficiently separated intermediate and small scales, the large scale magnetic helicity grows kinematically (independent of the magnetic Reynolds number) to approximately equal the sign and magnitude of the helicity injected on the intermediate scale. The oppositely signed magnetic helicity injected on the small scale subsequently drives a kinetic helicity driven dynamo through the secondary amplification of kinetic helicity. For the

driven case, in which the magnetic helicity injection is continuous,  $h_1$  grows beyond its kinematic value to a late time saturation value proportional to  $R_M$  for a closed or infinite system. For the free relaxation case, in which the driving is turned off, the secondary dynamo growth amplifies  $h_1$  only slightly beyond its kinematic growth value of  $h_2(0)/2$ , to a maximum value that is independent of  $R_M$  and  $\leq h_2(0)$ . A real astrophysical corona likely never reaches the  $R_M$  dependent regime as  $R_M$  is extremely large in practice. The magnitude of the large scale field growth taken from the end of the kinematic regime is then the most relevant. For bihelical injection of equal and opposite signs on the  $k_2$  and  $k_3$  scales, both injected with maximally helical fields, the ratio of magnetic energy on the large scale to that of the intermediate scale at the end of the kinematic regime is approximately  $k_1/k_2$ .

When the appropriate initial conditions are used, the solutions of the generalized equations also reproduce the results of the previously studied simpler cases of uni-helical magnetic relaxation<sup>13</sup> and the kinetic helicity driven dynamo.<sup>20, 21</sup>

In the context of magnetically dominated astrophysical coronae of stars or disks, bihelical magnetic helicity injection is natural because such coronae are fed with fields by velocity driven dynamos operating in their rotators below. Nonlinear helical velocity driven dynamos produce helical fields of opposite signs on different scales<sup>17, 23</sup> which can then emerge as bihelical fields into the corona. (Shear, not considered here, may effect the relative fraction injected on each scale<sup>55, 56</sup>.) The “large” scale and “small” scale of the rotator correspond to the “intermediate” and “small” scales of the corona respectively. The corona is therefore a natural environment for bihelical relaxation. The results herein suggest that helical large scale coronal fields can rapidly grow even when the coronae are injected with a net zero magnetic helicity. This is favorable for the in situ production of fields mediating coronal holes or MHD outflows from stars and disks.

Much more work is needed to incorporate the basic concepts and idealized solutions developed herein into realistic models of coronae. Shear, non-helical magnetic energy dynamics, and realistic boundary conditions should all be included.

Thanks to A. Brandenburg, G. Field, and E. Vishniac for related discussions and comments. DOE grant DE-FG02-00ER54600 and NSF grant AST-0406799 are acknowledged. Thanks also to KITP of UCSB, where this research was supported in part by NSF grant PHY99-07949.

1. H.K. Moffatt, *Magnetic Field Generation in Electrically Conducting Fluids*, (Cambridge University Press, Cambridge, 1978)
2. E.N. Parker, *Cosmical Magnetic Fields*, (Oxford: Clarendon Press, 1979)
3. F. Krause & K.-H. Rädler, *Mean-field Magnetohydrodynamics and Dynamo Theory*, (Pergamon Press, New York, 1980)
4. Ya. B. Zeldovich, A.A. Ruzmaikin, & D.D. Sokoloff, *Magnetic Fields in Astrophysics*, (Gordon and Breach, New York, 1983)
5. H.R. Strauss, Phys. Fluids, **28**, 2786 (1985)
6. H.R. Strauss, Phys. Fluids, **29**, 3008 (1986)
7. S. Ortolani & D.D. Schnack, *Magnetohydrodynamics of Plasma Relaxation* (World Scientific: Singapore, 1993)
8. A. Bhattacharjee & E. Hameiri, Phys. Rev. Lett. **57**, 206 (1986)
9. J.A. Holmes, B.A. Carreras, P.H. Diamond, & V.E. Lynch, Phys. Fluids, **31**, 1166 (1988)
10. A.V. Gruzinov & P.H. Diamond, Phys. Plasmas, **2**, 1941 (1995)
11. A. Bhattacharjee & Y. Yuan, Astrophys. J., **449**, 739 (1995)
12. P.M. Bellan, *Spheromaks*, (Imperial College Press, London, 2000)
13. E.G. Blackman and G. B. Field, Phys. Plasmas **11**, 3264 (2004)
14. H. Ji & S.C. Prager, Magnetohydrodynamics **38**, 191 (2002)
15. A. Pouquet, U. Frisch, J. Léorat, J. Fluid Mech., **77** 321 (1976)
16. N.I. Kleeorin & A.A. Ruzmaikin, Magnetohydrodynamics, **2**, 17, (1982)
17. E.G. Blackman, & G.B. Field, Mon. Not. R. Astron. Soc. **318**, 724 (2000)
18. A. Brandenburg, Astrophys. J., **550**, 824 (2001)
19. G.B. Field & E.G. Blackman, Astrophys. J., **572**, 685 (2002)
20. E.G. Blackman & G.B. Field, Phys. Rev. Lett., **89**, 265007 (2002)
21. E.G. Blackman & A. Brandenburg, Astrophys. J. **579**, 359 (2002)

- 22. E.G. Blackman, Mon. Not. R. Astron. Soc., **344**, 707 (2003)
- 23. E.G. Blackman & A. Brandenburg, Astrophys. J. Lett., **584** L99 (2003)
- 24. A. Brandenburg & W.H. Matthaeus, Phys. Rev. E., **69**, 056407 (2004)
- 25. J. Maron & E.G. Blackman, Astrophys. J. Lett. **566**, L41 (2002)
- 26. A. Brandenburg & K. Subramanian, “Astrophysical magnetic fields and nonlinear dynamo theory,” submitted to Phys. Rep., astro-ph/0405052, (2004)
- 27. A. Brandenburg, A. Bigazzi, K. Subramanian, Astron. Nachr. **323** 99 (2002)
- 28. J.B. Taylor, Rev. Mod. Phys., **58**, 741 (1986)
- 29. L. Golub & J. Pasachoff *Solar Corona*, (Cambridge: Cambridge Univ. Press, 1997)
- 30. G.L. Withbroe, & R.W. Noyes, Ann. Rev. Astron. Astrophys. **15**, 363, (1977)
- 31. C.J. Schrijver & C. Zwaan, *Solar and Stellar Magnetic Activity*, (Cambridge: Cambridge Univ. Press, 2000)
- 32. Y.-M. Wang & N.R. Sheeley, Astrophys. J., **599**, 1404 (2003)
- 33. A.A. Galeev, R. Rosner, G.S. Vaiana, Astrophys. J., **229** 318 (1979)
- 34. G.B. Field & R.D. Rogers, R.D. Astrophys. J., **403** 94 (1993)
- 35. F. Haardt & L. Maraschi, Astrophys. J., **413**, 507, (1993)
- 36. J. Wang, K. Watarai, & S. Mineshige, Astrophys. J. Lett., **607**, L107 (2004)
- 37. E.D. Feigelson, & T. Montmerle, Ann. Rev. Astron. Astrophys., **37**, 363 (1999)
- 38. S.H. Lubow, J.C.B. Papaloizou, J.E. Pringle, Mon. Not. R. Astron. Soc., 267, 235 (1994).
- 39. E.G. Blackman & J.C. Tan, Astrophys. & Space Sci., in press (astro-ph/0306424)
- 40. R.D. Blandford & D.G. Payne, Mon. Not. R. Astron. Soc., **199**, 883 (1982)
- 41. R.V.E. Lovelace, J.C.L. Wang, & M.E. Sulkkanen, M.E. Astrophys. J., **315**, 504 (1987)
- 42. D.L. Meier, S. Koide, & Y. Uchida, Science, **291**, 84 (2001)
- 43. R. Ouyed, D.A. Clarke, & R.E. Pudritz, Astrophys. J., **582** 292 (2003)

- 44. S. Koide, *Astrophys. J. Lett.*, **606**, L45 (2004)
- 45. C.G. Campbell, *Mon. Not. R. Ast. Soc.*, **306**, 307 (2000)
- 46. B. Von Rekowski & A. Brandenburg, *Astron. & Astrophys.*, **420**, 17 (2004)
- 47. R.V.E. Lovelace, H. Li, A.V. Koldoba, G.V. Ustyugova, & M.M. Romanova, *M. M. Astrophys. J. Lett.*, **572**, 445 (2002)
- 48. K.A. Miller and J.M. Stone, *Astrophys. J. Lett.*, **534**, 398 (2000)
- 49. R.E. Pudritz, *Mon. Not. R. Astron. Soc.*, **195**, 897 (1981)
- 50. M. Reyes-Ruiz, & T.F. Stepinski, *T. F. Mon. Not. R. Astron. Soc.*, **285**, 501 (1997)
- 51. M. Reyes-Ruiz, & T.F. Stepinski, *Astron. & Astrophys.*, **342**, 892 (1999)
- 52. T.A. Yousef & A. Brandenburg, *Astron. & Astrophys.*, **407**, 7 (2003).
- 53. L. Woltjer, *Proc. Nat. Acad. Sci.*, **44**, 489 (1958)
- 54. M.A. Berger & G.B. Field, *J. Fluid Mech.*, **147**, 133 (1984)
- 55. E.T. Vishniac, & J. Cho, *Astrophys. J* **550**, 752 (2001)
- 56. A. Brandenburg & C. Sandin, “Catastrophic alpha quenching alleviated by helicity flux and shear,” submitted to *Astron. & Astrophys.* (2004)

**Figure 1:** Driven bihelical magnetic relaxation for  $c_1 = 0$ . Here  $h_2 = -h_3 = 1$ , for all time,  $k_1 = 1$ ,  $k_2 = 5$ ,  $k_3 = 20$  and  $h_1(t = 0) = 0.01$ . (a)  $h_1$ , where  $R_M = R_V = 1000$  (dashed)  $R_M = R_V = 6000$  (solid). The saturation value of  $h_1$  depends linearly on  $R_M$ . (b) Same as (a) but for early times. The kinematic regime ends where the two curves split. Note that just after the kinematic regime the  $R_M = 6000$  curve is below that of  $R_M = 1000$  in contrast to the late-time regime in (a). (c)  $h_2$  (short dashed, straight line) and  $h_2^V$  (long dashed). The curves for  $R_M = 6000$  and  $R_M = 1000$  indistinguishably overlap. (d)  $h_3$  (straight dashed line) and  $h_3^V$  (oscillating solid line). Again negligible variation for  $R_M = 1000$  and  $R_M = 6000$  cases. (e) Dimensionless EMFs:  $\overline{Q}$  (solid humped curve),  $\overline{q}$  (long dashed), and  $q_2$  (short dashed) for  $R_M = 1000$ . (f)  $h_1$  when  $h_3^V \ll 1$  is artificially enforced for  $R_M = 1000$ , and multiplying the  $q_2$  term in (34) by 1 (dashed) and 0.5 (solid) to show the relative effect on  $h_1$ .

**Figure 2:** Same as Fig. (1a) but with different values of the  $h_1$  loss coefficient  $c_1$ , and  $h_1(0)$ . (a)  $c_1 = 0.1$ ,  $h_1(0) = 0.01$  (b)  $c_1 = 1$ ,  $h_1(0) = 0.01$ . These late time curves are insensitive to the choice of  $h_1(0)$ .

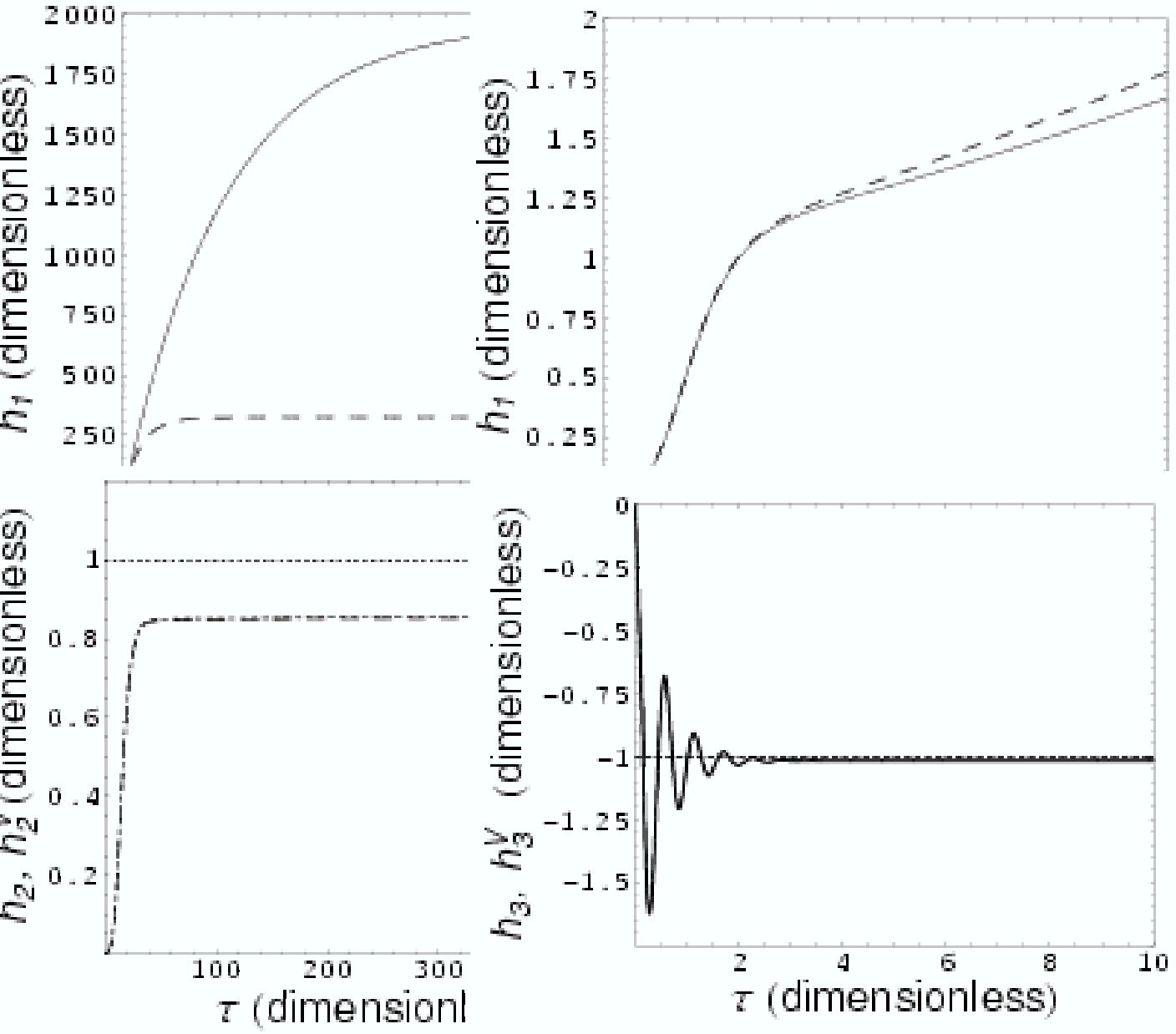
**Figure 3:** Kinetic helicity driven dynamo. Here the system is driven such that  $h_2^V = 1$  for all times, and a seed  $h_1(0) = 0.01$ . These curves show that Eqs. (31-38) reproduce the results of Ref. 21 for the appropriate initial conditions. (a) Late time solution of  $h_1$  for  $R_M = R_V = 1000$  (dashed) and  $R_M = R_V = 6000$  (solid). (b) early time solution for  $h_1$ .

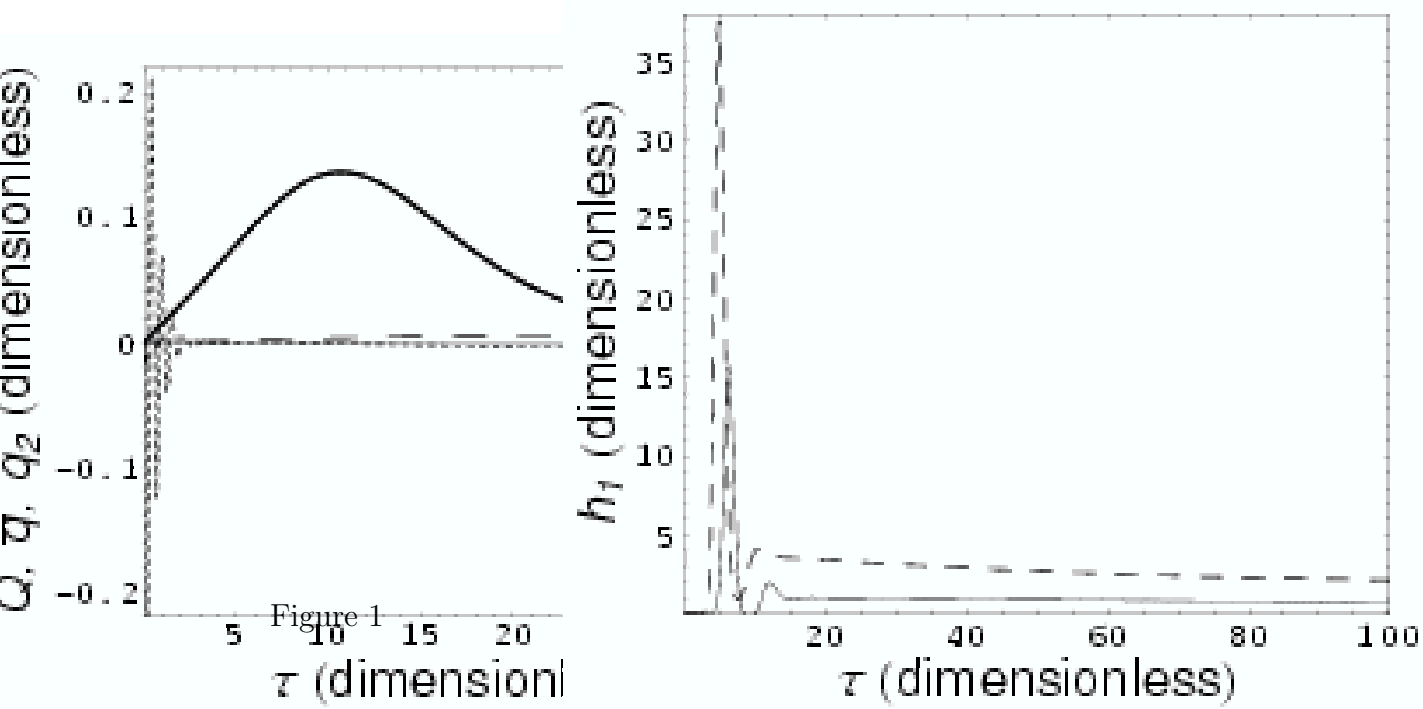
**Figure 4:** Unihelical magnetic relaxation. Here the system is driven with  $h_2 = 1$  and  $h_3 = 0$  for all times, with a seed  $h_1(0) = 0.01$ . These curves show that the generalized set of equations reproduces unihelical relaxation of Ref. 13. (a)  $h_1$  for  $R_M = R_V = 1000$  (dashed) and  $R_M = R_V = 6000$  (solid). (b) same as (a) but at early times (c)  $h_1$  for  $R_M = R_V = 1000$  (solid) and  $R_M = 10R_V = 1000$  (dashed) (d) same as (c) for early times.

**Figure 5:** Free bihelical magnetic relaxation. Here  $h_1(0) = 0.01$ ,  $h_2(0) = -h_3(0) = 1$  but unlike the case of Fig. 1, there is no subsequent driving. (a)  $h_1$ , where  $R_M = R_V = 2000$  (dotted)  $R_M = R_V = 10000$  (dashed) and  $R_M = 10000$  and  $R_V = 2000$  (solid). Note the slower decay for larger  $R_M$  and  $R_V$ . (b) Same as (a) for early times. Note the insensitivity to  $R_V$  at these times since the dotted and solid curves defined in (a) overlap. (c)  $h_2$  for  $R_M = R_V = 2000$  (thin solid);  $h_2^V$  for  $R_M = R_V = 2000$  (short-dashed);  $h_2$  for  $R_M = R_V = 10000$  (thick solid);  $h_2^V$  for  $R_M = R_V = 10000$  (long-dashed). Note that  $h_2$  initially decays and  $h_2^V$  rises and then the curves decay together. The solutions for  $h_2$  and  $h_2^V$  are insensitive to  $R_V$  for a given  $R_M$ . Note that  $h_2$ ,  $h_2^V$  actually deplete faster for larger  $R_M$  (see (e) and text). (d)  $h_3$  and  $h_3^V$ . At early times (barely visible),  $|h_3|$  decays and  $|h_3^V|$  increases

and then the curves nearly overlap in decay:  $h_3$  and  $h_3^V$  for  $R_M = R_V = 2000$  (top);  $h_3$  and  $h_3^V$  for  $R_M = R_V = 10000$  (bottom)  $h_3$  and  $h_3^V$  for  $R_M = 10000$ ,  $R_V = 2000$  (middle). (e) Blow-up of (d) to show the offset between  $h_3^V$  and  $h_3$  with the  $h_3^V$  curves are the solid curves on the right of each pair, and  $h_3$  is the left dashed curve in each pair. The pairs from left to right are  $h_3$  and  $h_3^V$  for  $R_M = R_V = 2000$ ;  $h_3$  and  $h_3^V$  for  $R_M = R_V = 10000$ ;  $h_3$  and  $h_3^V$  for  $R_M = 10000$ ,  $R_V = 2000$ . The offset accounts for the weak  $h_3^V$  driven dynamo that grows  $h_1$  slightly beyond its  $h_1 = 1/2$  kinematic growth value. (f) Dimensionless EMFs:  $\bar{q}$  for  $R_M = R_V = 10000$  (thick solid),  $\bar{q}$  for  $R_M = R_V = 2000$  (long dashed),  $q_2$  for  $R_M = R_V = 10000$  (thin solid),  $q_2$  for  $R_M = R_V = 2000$  (short dashed).







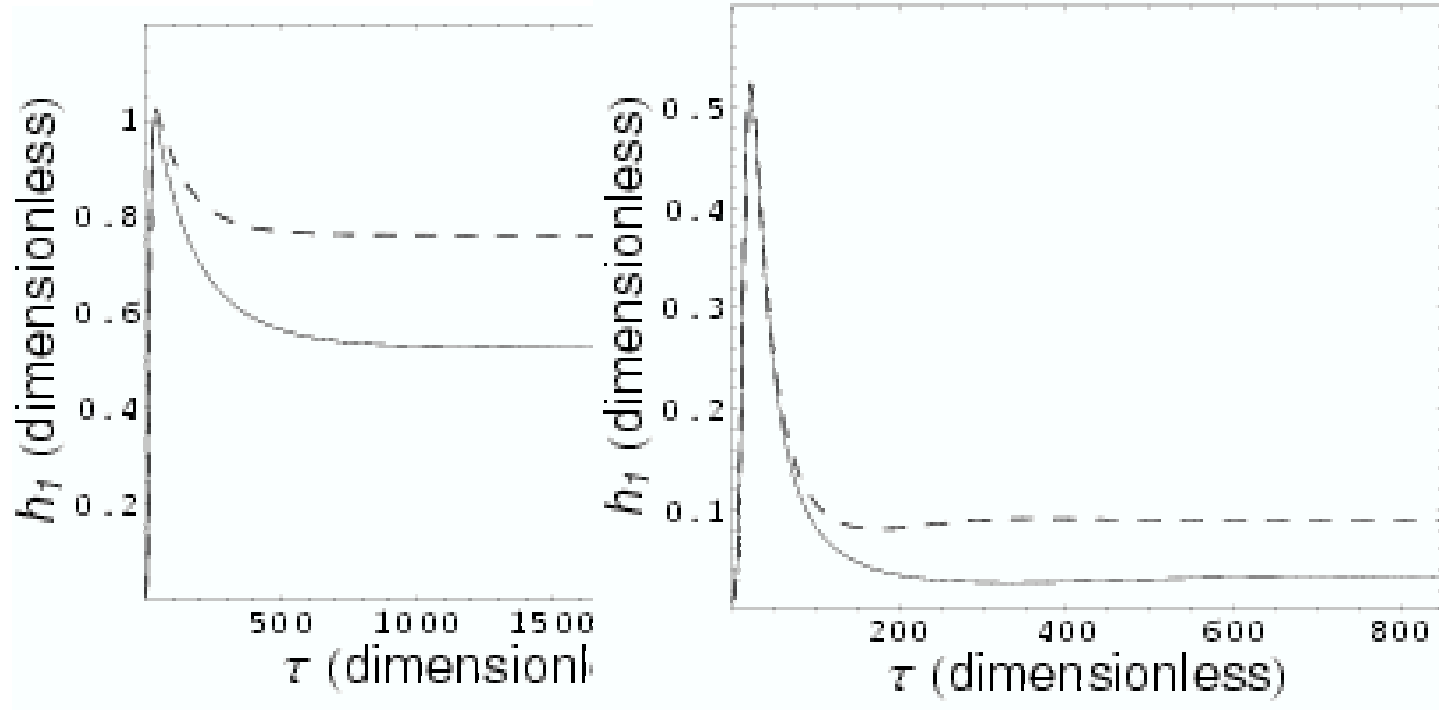


Figure 2

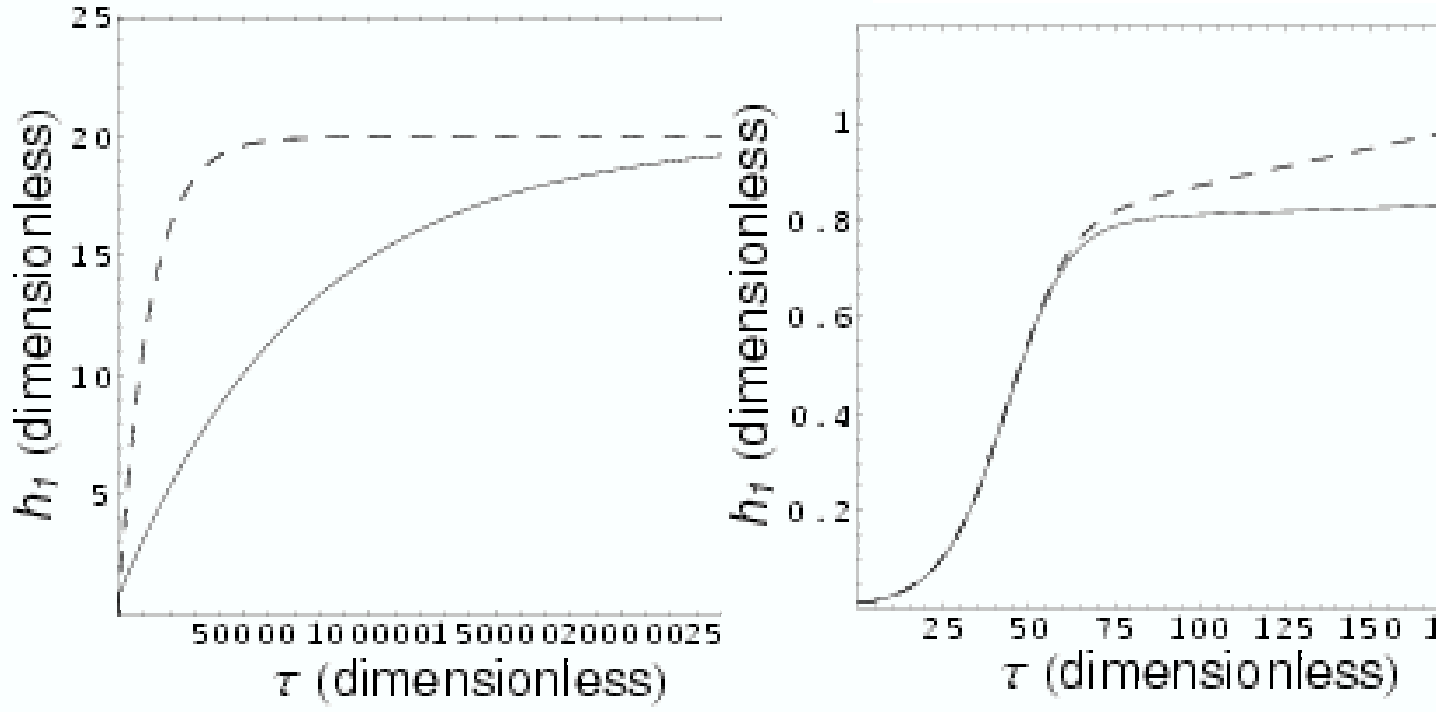


Figure 3

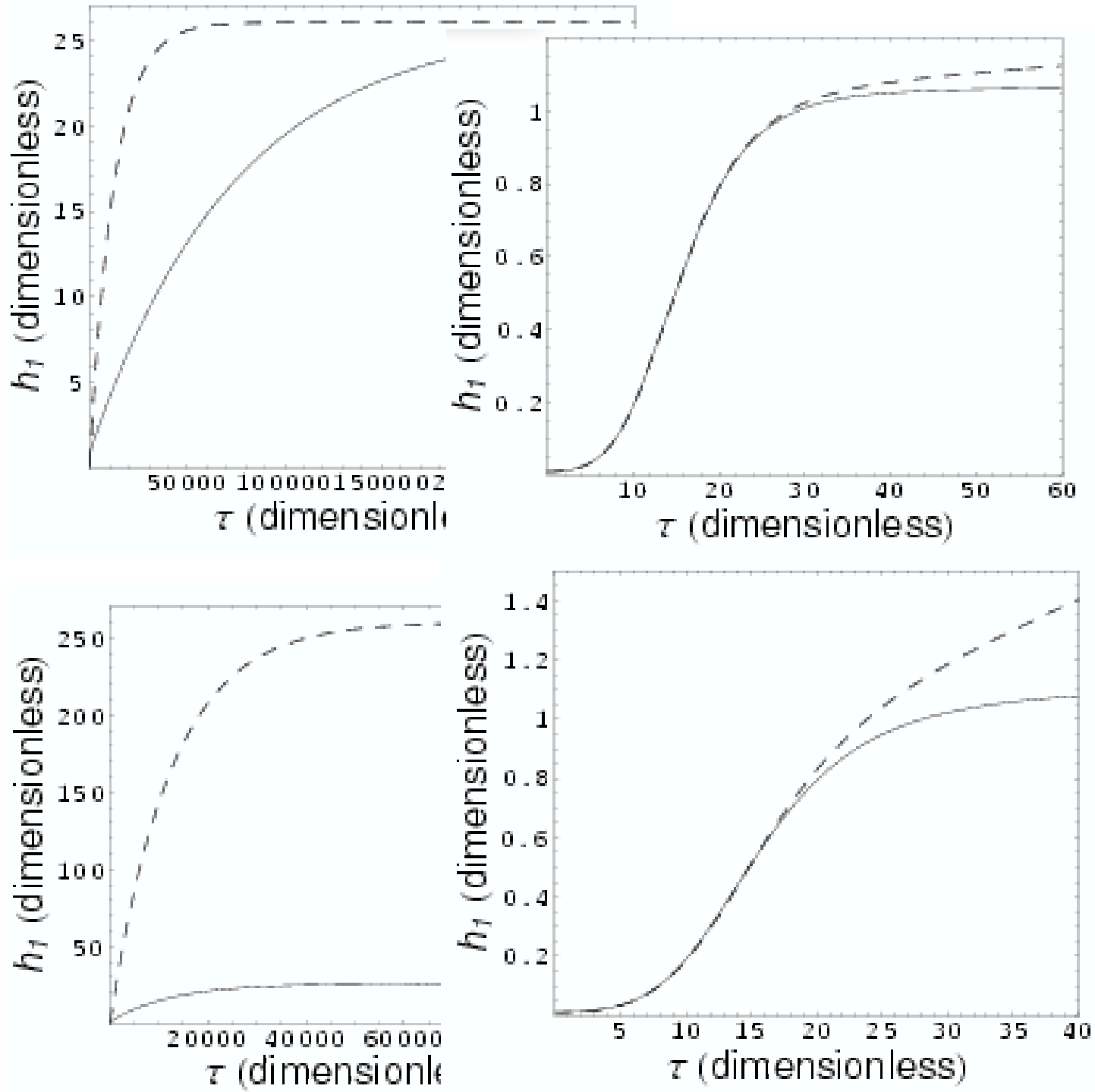


Figure 4

